A Hybrid MAV for Ingress and Egress of Urban Environments

William E. Green and Paul Y. Oh

***Abstract*—Small bird-sized aerial robots are expendable and can fly over obstacles and through small openings to assist in the acquisition and distribution of intelligence during reconnaissance, surveillance, and search-and-rescue missions in urban environments. However, limited flying space and densely populated obstacle fields require a vehicle that is capable of hovering but is also maneuverable. A secondary flight mode was incorporated into a fixed-wing aircraft to preserve its maneuverability while adding the capability of hovering. An inertial measurement sensor and onboard flight control system were interfaced and used to transition the hybrid prototype from cruise to hover flight and sustain a hover autonomously. Furthermore, the hovering flight mode can be used to maneuver the aircraft through small openings such as doorways. An ultrasonic and infrared sensor suite was designed to follow exterior building walls until an ingress route was detected. Reactive control was then used to traverse the doorway and gather reconnaissance. This paper describes the holistic approach of platform development, sensor suite design, and control of the hybrid prototype.**

***Index Terms*—Collision avoidance, field service robotics, hovering, navigation, unmanned aerial vehicles.**

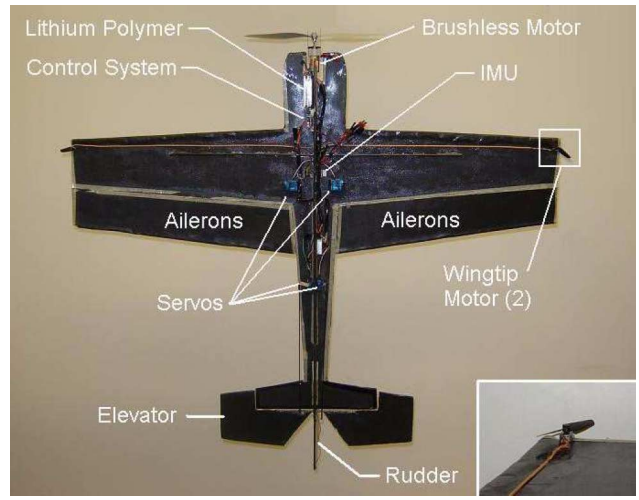

Fig. 1. Our fixed-wing prototype is shown in its hovering orientation. (Inset) Motors on the wingtips are added to counter the effects of motor torque.

I. Introduction

DISASTERS that occur in near-Earth environments, such as subway tunnels, train stations, or urban structures, can cripple or deny access to command and control teams. This makes acquiring situational awareness without the use of aerial vehicles virtually impossible. This was evidenced during Hurricane Katrina, when flooded streets prevented ground-based vehicles from gaining access. Instead, a team from the University of South Florida's Center for Robot Assisted Search and Rescue utilized miniature unmanned helicopters to help survey damage and assess the structural integrity of buildings. These types of small unmanned aircraft can be rapidly deployed to gather intelligence in such environments.

Even smaller aircraft, or micro air vehicles (MAVs), range in size from flying insect [3] or bird-sized platforms [9] to slightly larger vehicles such as DARPA's organic air vehicle. Vehicles of this magnitude can easily fit through small openings such as windows or doorways, making them ideal for near-Earth environments. However, without line-of-sight for manual or semiautonomous control, missions must be performed autonomously. This is a major challenge since current sensing technologies are not mature enough for such autonomy. Furthermore, cluttered flying environments make conventional cruise flight extremely challenging. As such, a hovering vehicle with high maneuverability is preferred.

Leveraging a maneuver known as *prop-hanging* from the radio-controlled airplane community, the authors were able to integrate the maneuverability and endurance superiority of fixed-wing aircraft with hovering capabilities of rotary-wing vehicles [5]. During a prop-hang, where the fuselage is completely vertical, the thrust from the motor and propeller balance the weight of the aircraft (see Fig. 1). This is made possible by a high thrust-to-weight ratio ($T/W > 1$), which also allows a quick transition from cruise flight, through the stall regime, and into hovering mode. However, the aircraft is unstable in this configuration and requires an expert human pilot to constantly manipulate the aircraft's control surfaces (e.g., rudder and elevator) in order to sustain a vertical orientation. With full autonomous operation in mind, taking the human out of the loop during this difficult and demanding flight mode is a logical first step. An onboard control system was used to acquire data from an orientation sensor to automate the process.

This paper illustrates the usefulness of a hovering, fixed-wing aircraft for flight in cluttered terrain. Section II discusses the evolution of the most recent prototype and explains the transition from cruise-to-hover (CTH) flight. Section III presents the quaternion attitude control algorithm, while Section IV details the attitude sensor and controller used to achieve autonomous

Manuscript received January 21, 2008; revised June 12, 2008. Current version published April 3, 2009. This paper was recommended for publication by Associate Editor D. Sun and Editor H. Arai upon evaluation of the reviewers' comments. This work was supported by the National Science Foundation under Grant 0347430.

W. E. Green is with Avionics and Software Department, Alliant Techsystems, Minneapolis, MN, USA (e-mail: william.e.green@drexel.edu).

P. Y. Oh is with Drexel Autonomous Systems Laboratory, Drexel University, Philadelphia, PA 19104 USA (e-mail: paul.yu.oh@drexel.edu).

Color versions of one or more of the figures in this paper are available online at http://ieeexplore.ieee.org.

Digital Object Identifier 10.1109/TRO.2009.2014501

1552-3098/$25.00 © 2009 IEEE

hovering. Section V discusses the experimental results. The paper finishes with sections on future work and conclusions.

II. Platform Evolution

Reconnaissance missions in tunnels or inside buildings demand a small-scale aircraft that is highly maneuverable. The initial prototype weighed 30 g, had a 46 cm (18 in) wingspan, and could fly for 20 min on a 145 mA·h lithium polymer battery. It was maneuverable in the sense that it flew so slowly (approximately 2 m/s), oncoming collisions were detected and avoided well before the aircraft got there. With a 15-g payload, optic flow microsensors [1] were mounted on the front of the plane and were used to perform autonomous collision avoidance maneuvers inside an urban structure [5]. However, the small payload capacity of the aircraft was quickly exhausted. Furthermore, the lightweight airframe prevented flight outdoors. As such, the design specifications were modified such that the next generation was

1) highly maneuverable;
2) compact (less than 91 cm, or 3 ft)
3) capable of flying 25 min or longer
4) able to carry a payload of 100 g
5) capable of hovering.

The revised design specifications narrowed the list of feasible platforms down to two configurations: fixed- and rotary-wing. Neither platform, however, was able to meet all five design parameters. For example, fixed-wing platforms leverage the lift generated from airfoils to provide longer flight times, but are unable to hover. Rotary-wing aircraft, such as helicopters and ducted fans [2], [7], are capable of stationary flight but have limited endurance because the lift is provided directly by electric or gas-powered motors. However, constant hover is not always necessary. Peeping inside a cave or tunnel may be required for only a small percentage of the overall mission. Fixed-wing aircraft are able to perform rapid dash maneuvers and fly for longer times. Also, the idea of a "retrofit," and so existing fixed-wing aircraft, can hover may be attractive; new vehicles would not need to be procured. Instead, a hovering feature can just be added. It therefore seemed logical to develop a hybrid in order to meet all of the design specifications.

A. Hybrid Platform

With a maneuver adopted from the radio-controlled airplane community known as prop-hanging, adding an additional flight modality to a fixed-wing aircraft was realizable. Prop-hanging is the aircraft's ability to balance its weight with the thrust generated from the propeller. In order to transition into and sustain a hover by prop-hanging, a thrust-to-weight ratio greater than one is required. With a weight estimate of 600 g, as shown in Table I, a brushless motor was selected, which can generate more than 1000 g of thrust (i.e., a $T/W = 1.67$). Another design factor is that the aircraft must be controlled with limited airflow (i.e., prop wash) over the control surfaces once in the hovering position. As a result, the control surface areas of the vertical and horizontal tails and wing must also be increased. The net result is that a small drag force can be used to regulate rotation about all three axes.

TABLE I
MAV Weight Distribution

Part Description	Weight (grams)
Carbon Fiber Airframe	324
Motor, Gearbox, and Prop	85
Servos (4)	36
Lithium-Poly Battery	85
Speed Controller and Receiver	25
Inertial Measurement Unit	26
Onboard Control System	18
Total	599

The unique capabilities of the prototype make it extremely difficult for a human pilot to fly. The pilot must have experience of flying both fixed- and rotary-wing aircraft and must also have a feel for how the rudder and elevator deflection mimic a helicopter's cyclic control. The following section describes how a human pilot transitions between the cruise and hover flight modes and also how hovering is sustained.

B. Transitioning Between Flight Modes

The most critical aspect of the hybrid design is the transition from CTH flight, which can also be used as a secondary collision avoidance maneuver (see Fig. 2). During this phase, there exists an angle-of-attack α for which the wings are no longer a contributing factor to the lift component (i.e., stall). To achieve the transition, the aircraft has to leverage its momentum and essentially overpower its way through the stall regime. The high thrust-to-weight ratio built into the design helps to ensure that the momentum is not lost through the transition. Furthermore, as the aircraft is transitioning from cruise flight (minimum thrust) to the hovering flight mode, the throttle must be increased to balance the weight of the aircraft. The transition back to cruise mode first requires vertical acceleration to give the plane some momentum and then the elevator is deflected to pitch the aircraft forward into cruise mode. However, there may be circumstances when a vertical acceleration is not feasible (e.g., indoors with a low ceiling). In this case, the aircraft can be pitched forward first and then given increased throttle to pull out of stall.

C. Hovering

After transitioning into the hovering mode, the attitude must be sustained by constantly adjusting four channels of a radio-controlled transmitter. The most critical task the expert human pilot has is to maintain the aircraft's vertical orientation by adjusting the rudder and elevator deflection angles. Also, the throttle position must be modified to balance the weight of the aircraft. Once the stick position is found to hold the plane at a constant altitude, it remains relatively constant as the aircraft is not gas powered and therefore maintains the same weight throughout the flight. Finally, the MAV's reaction to the motor torque results in the plane rotating about the vertical axis when hovering. This is known as torque rolling and can sometimes be

Fig. 2. Our MAV prototype with a 1m wingspan manually transitions from (left) cruise flight through (middle) the stall regime and into a (right) hovering position to avoid a collision with a basketball net.

countered with aileron control. All of these efforts must be done simultaneously, which makes hovering a challenging task.

III. Attitude Control

There are many different ways to represent the attitude of a rigid body in 3-D space. However, most methods are either vulnerable to singularities at critical orientations (e.g., an Euler pitch angle equal to 90°) or computationally inefficient when representing rotations. To avoid these drawbacks, a quaternion attitude controller is developed for the transition from CTH flight and then to sustain a hover.

A. Quaternions

Quaternions provide a means of representing attitude and performing transformations between orthogonal, Cartesian coordinate systems [11]. They are most commonly used in the spacecraft, [13], [14] and gaming industries [10]. The value of quaternions can be attributed to their compactness and freedom from singularities. The characteristics of quaternions make them ideal for representing the orientation of vehicles that perform large angular maneuvers such as spacecraft. Although they are rarely used for attitude control of fixed-wing aircraft, quaternions serve as a promising approach for regulating the hovering flight mode of the hybrid prototype.

A quaternion consists of four parameters. The first three components represent the vector part of the quaternion and the fourth component represents the scalar portion. They are defined by

$$q_1 = e_x \sin\left(\frac{\Theta}{2}\right) \tag{1}$$

$$q_2 = e_y \sin\left(\frac{\Theta}{2}\right) \tag{2}$$

$$q_3 = e_z \sin\left(\frac{\Theta}{2}\right) \tag{3}$$

$$q_4 = \cos\left(\frac{\Theta}{2}\right) \tag{4}$$

where e_x, e_y, and e_z represent the eigenaxes, or Euler axes, and Θ gives the scalar angle of rotation about that axis. The eigenaxis is multiplied by the sine of half the rotation angle and the cosine of this angle is taken to represent the scalar component. Furthermore, the products of quaternions can be used to represent rotations from one coordinate frame to another.

B. Hovering Control Algorithm

The autonomous hovering algorithm begins by defining the commanded quaternion q_c that describes the MAV's orientation during a hover (i.e., vertical with belly facing north in a NED coordinate frame). The rotation is about the y-axis and, thus, the eigenaxis is represented by

$$(e_x, e_y, e_z) = (0, 1, 0). \tag{5}$$

With a rotation angle of 90°, the quaternion representation of this attitude is given by

$$q_{c_1} = e_x \sin\left(\frac{\Theta}{2}\right) = 0 * \sin\left(\frac{\pi}{4}\right) = 0.000i$$

$$q_{c_2} = e_y \sin\left(\frac{\Theta}{2}\right) = 1 * \sin\left(\frac{\pi}{4}\right) = 0.707j$$

$$q_{c_3} = e_z \sin\left(\frac{\Theta}{2}\right) = 0 * \sin\left(\frac{\pi}{4}\right) = 0.000k$$

$$q_{c_4} = \cos\left(\frac{\Theta}{2}\right) = \cos\left(\frac{\pi}{4}\right) = 0.707.$$

The commanded quaternion is used as the input into the control algorithm, as seen in Fig. 3. Once the commanded quaternion is defined, the error quaternion can be calculated using the following formula:

$$q_e = q_m^* \otimes q_c \tag{6}$$

where q_m^* represents the conjugate of the measured quaternion that is acquired with an attitude sensor [e.g., inertial measurement unit (IMU)] mounted onboard the aircraft. Equation (6) defines the error quaternion in the body frame of the aircraft. Once the error quaternion is calculated, the angular error about the x, y, and z axes can be extracted from q_e by first normalizing the vector component and then multiplying by the angle

$$\begin{aligned} E_x &= 2\cos^{-1}(q_{e_4})\, q_{e_1}/\|q_{e_v}\| \\ E_y &= 2\cos^{-1}(q_{e_4})\, q_{e_2}/\|q_{e_v}\| \\ E_z &= 2\cos^{-1}(q_{e_4})\, q_{e_3}/\|q_{e_v}\| \end{aligned} \tag{7}$$

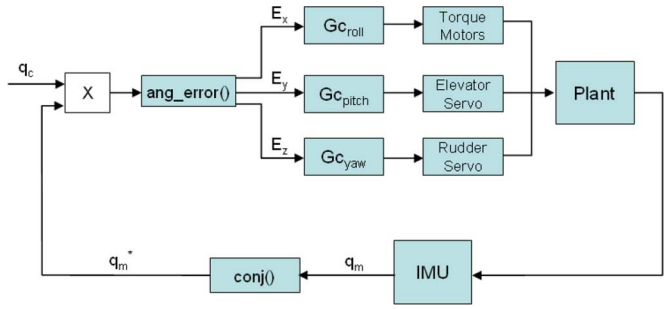

Fig. 3. Block diagram of three compensators for roll, pitch, and yaw.

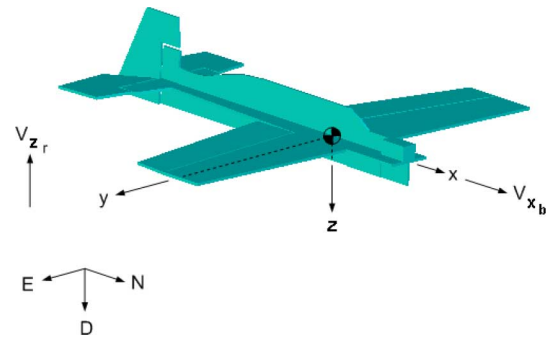

Fig. 4. Vertical vector in the reference frame is shown along with the x-axis vector in the body frame.

where $\|q_{e_v}\|$ is the norm of the vector part of the error quaternion. When (7) is applied to the error quaternion from before, it yields the angular error about each axis. These angular errors are fed into the roll, pitch, and yaw controllers ($Gc_{\rm roll}$, $Gc_{\rm pitch}$, and $Gc_{\rm yaw}$, as seen in Fig. 3). Several compensators were evaluated for attitude control, but proportional derivative (PD) controllers seemed to be the most robust and effective. The output of the roll, pitch, and yaw compensators was then fed into the torque control, elevator, and rudder servos, respectively. This, in turn, drives the aircraft orientation back to the hovering attitude. Although this algorithm seems to work effectively when the aircraft starts from orientations close to vertical, it was soon realized that it is not optimal for the transition from CTH flight.

C. CTH Control Algorithm

The hovering error quaternion assumes that the aircraft is in a near-hovering orientation when the algorithm is initiated. In this case, the orientation of the aircraft's belly does not affect the algorithm, that is, if the belly of the aircraft faces east, south, or west, the controller will command the plane to the vertical orientation while simultaneously rolling the aircraft until the belly faces north. However, when starting from cruise flight, this same algorithm will result in a large control effort about more than one axis if the aircraft is heading in a direction other than north (i.e., if heading north, it will just result in a pitch up maneuver). While this maneuver will most likely work, it was desired to have a pure pitching motion to transition from CTH when heading in any direction, i.e., if the aircraft is in cruise mode heading south, the transition from cruise flight to hover mode should leave the aircraft in the vertical orientation with the belly facing south. This method was desired because it primarily required control about a single axis rather than two axes simultaneously. Furthermore, when put into practical use, the aircraft will most likely be flying toward its target with a camera mounted on the belly of the airframe. Ideally, the aircraft would pitch up and have the belly still facing the target. To achieve this, a delta quaternion is introduced, which generates a new commanded quaternion based on the aircraft's heading when the CTH algorithm is initialized.

When the transition from CTH is initialized, there is an angular error between the x-axis of the aircraft and a vertical vector expressed in the reference frame. Assuming perfect cruise conditions (i.e., $\phi = 0$, $\theta = 0$, and $-180 \leq \psi \leq 180°$), this error is equal to 90° about the pitch axis. As mentioned before, the commanded quaternion for hovering cannot be used because it will not result in the desired pitch-up maneuver to reach the vertical orientation [8]. Instead, vector and quaternion mathematics will be used to generate a delta quaternion that represents a rotation from the initial aircraft attitude in quaternion form to the vertical orientation. Using the delta and measured quaternions, a commanded quaternion can then be calculated, which represents the vertical orientation with the belly facing the same direction as the aircraft was heading when the algorithm was initialized. Upon obtaining the commanded quaternion, the error quaternion can then be computed for each new measured quaternion (i.e., each control loop iteration), which will generate a pure pitching maneuver despite the initial aircraft heading.

Assuming the CTH algorithm has been initialized and the first measured quaternion has been acquired, the process to calculate the delta quaternion starts by defining the vertical vector in the reference (NED) frame V_{z_r}

$$V_{z_r} = 0.0i + 0.0j - 1.0k \tag{8}$$

and the aircraft's x-axis in the body frame V_{x_b}, as seen in Fig. 4

$$V_{x_b} = 1.0i + 0.0j + 0.0k. \tag{9}$$

It is desired to keep the error quaternion in the aircraft's body frame such that the angular errors can be directly used to control the aileron, elevator, and rudder surfaces. Therefore, all calculations will be performed in the body frame. As such, the first step is to transform the vertical vector (V_{z_r}) from the reference frame to the body frame using the measured quaternion. This is performed by

$$V_{z_b} = q_m^* \otimes V_{z_r} \otimes q_m \tag{10}$$

where V_{z_b} represents V_{z_r} transformed to the body frame. It should be noted that in the previous equation, V_{z_r} is first converted to a 4-tuple by adding a zero to act as the scalar component. This is done to make it compatible with quaternion multiplication. V_{z_b} is then converted back to a vector by removing the scalar portion of the resulting 4-tuple.

Now that the vertical vector and the aircraft's x-axis are both represented in the body frame, vector mathematics can be used to find an orthogonal rotation axis and angle between the two

vectors. The cross product is calculated to find the rotation axis, or the axis that is orthogonal to both vectors

$$V_{\text{rot}} = V_{x_b} \times V_{z_b}. \tag{11}$$

Next the angle between the MAV's x-axis and vertical vector in the body frame can be found by using the dot product

$$\gamma = \cos^{-1}(V_{x_b} \cdot V_{z_b}). \tag{12}$$

The axis and angle representing the rotation to have the aircraft's x-axis coincide with the vertical vector are now known and can be converted into a quaternion, which will be referred to as the delta quaternion q_Δ

$$q_{\Delta_1} = V_{\text{rot}_1} \sin\left(\frac{\gamma}{2}\right) \tag{13}$$

$$q_{\Delta_2} = V_{\text{rot}_2} \sin\left(\frac{\gamma}{2}\right) \tag{14}$$

$$q_{\Delta_3} = V_{\text{rot}_3} \sin\left(\frac{\gamma}{2}\right) \tag{15}$$

$$q_{\Delta_4} = \cos\left(\frac{\gamma}{2}\right). \tag{16}$$

The newly calculated delta quaternion q_Δ and the first measured quaternion from (10) can be used to calculate the new commanded quaternion q_c'

$$q_c' = q_m \otimes q_\Delta. \tag{17}$$

The new commanded quaternion represents the vertical orientation with the belly of the aircraft facing in the same direction as the heading in cruise mode. The entire process to calculate q_c' is performed once at the initialization of the CTH maneuver. The resulting commanded quaternion remains constant and is used in every iteration along with a new measured quaternion to compute the error quaternion. The equation for the error quaternion (6) is restated as

$$q_e = q_m^* \otimes q_c'. \tag{18}$$

Finally, since the error quaternion is calculated in the body frame of the aircraft, the angular error about each axis can be used to control the aileron, elevator, and rudder surface deflection. The angular errors are calculated using the relationships from (7)

$$E_x = 2\cos^{-1}(q_{e_4})\, q_{e_1}/\|q_{e_v}\|$$
$$E_y = 2\cos^{-1}(q_{e_4})\, q_{e_2}/\|q_{e_v}\|$$
$$E_z = 2\cos^{-1}(q_{e_4})\, q_{e_3}/\|q_{e_v}\|.$$

Again, the angular errors about each axis can be used in a PD control scheme to generate aileron, elevator, and rudder deflections, as in Section III-B:

$$\delta_e = K_{p_e} E_y + K_{d_e} \dot{E}_y \tag{19}$$

$$\delta_r = K_{p_r} E_z + K_{d_r} \dot{E}_z. \tag{20}$$

IV. Sensing and Control Hardware

Automating the hovering flight mode requires that the aircraft attitude be measured. Furthermore, this attitude must be in quaternion form in order for the algorithm of Section III to be implemented.

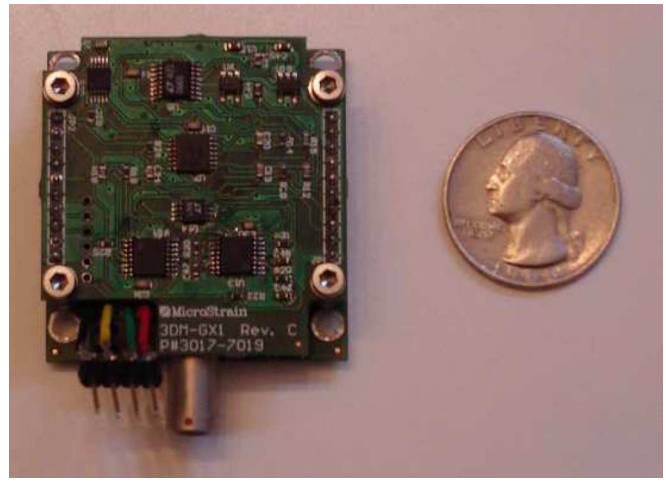

Fig. 5. Microstrain's 30-g IMU sensor was used to feedback attitude information to the onboard control system.

A. Inertial Measurement Unit (IMU)

Autonomous control of the hybrid prototype requires an inertial sensor capable of measuring aircraft attitude during unconventional maneuvers and orientations. The two most critical parameters are the output mode and gyro range capabilities of the sensor. Typically, the gyro range is specified at 150 or 300°/s for most MEMs gyros. The speed of the transition from CTH was measured at 120°/s with a low end sensor. Therefore, an IMU with a gyro range of at least 150°/s was required.

Using this specification and a desired output mode in quaternion form, a Microstrain 3DM-GX1 inertial measurement unit was selected. Fig. 5 shows the Microstrain IMU, which outputs a gyroscopically stabilized four component quaternion describing the MAV's orientation with respect to the fixed-Earth coordinate frame. It weighs just 30 g out of its protective casing and comprises three triaxial accelerometers and angular rate gyros as well as three orthogonal magnetometers. The gyro range is 300°/s, which is more than enough to handle the transition from CTH flight. It filters the data onboard and sends the digitized attitude data via RS-232 protocol at a rate of 100 Hz.

B. Flight Control System (FCS)

The FCS's microcontroller has several responsibilities including acquiring attitude data from the IMU, implementing the control algorithm for autonomous hovering or the transition into hover mode, and generating the corresponding pulsewidth modulated (PWM) servo signals to control the amount of aileron, elevator, and rudder deflection. Microchip's PIC18F8722 was selected for the FCS because it had the largest amount of program (e.g., 128 KB) and data (e.g., 3.9 KB) memory of all the 8-bit microcontrollers, multiple capture-compare-PWM pins to decode PWM signals, several RS-232 transmit and receive pins, I2C capabilities to write data to external memory, and surface mount packaging to reduce size and weight. Other FCS

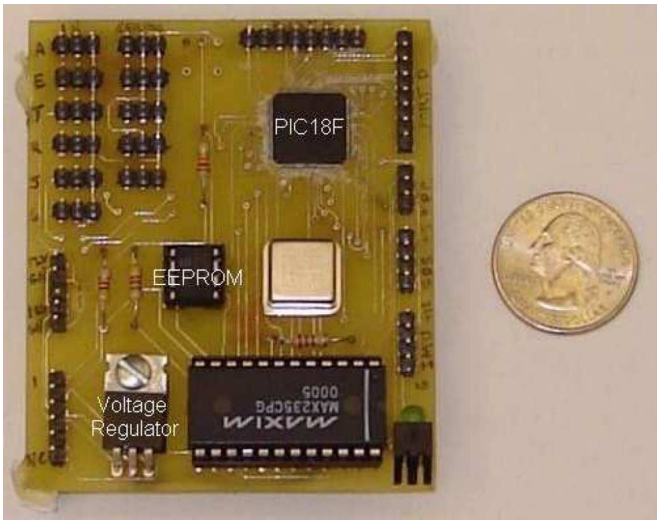

Fig. 6. Twenty-five-gram FCS was developed for controlling the hybrid prototype.

components include a 10-MHz external clock, an RS-232 converter chip for communication with the IMU sensor, and 65 KB of external nonvolatile memory.

Attitude data for each flight are sent to an EEPROM chip via I2C communication and are downloaded and analyzed postflight. Also, the FCS was designed to be modular and includes six input and five output ports for connecting servos or other DC motors. Therefore, it can easily be disconnected from one air or ground vehicle and used as the control system for another by simply reprogramming the microcontroller. The complete system weighs 25 g and is shown in Fig. 6.

V. Experiments

The first autonomous hovering experiments were conducted inside an urban structure, with limited flying space, (i.e., $1 \times 1\,\mathrm{m}^2$ area). Also, another indoor experiment was performed to contrast the differences in stability between manual and autonomous hovering.

A. Autonomous Hovering

The aircraft was released in near-hovering orientation (i.e., the fuselage is close to vertical) and manually given enough throttle to balance the aircraft weight. The controls are simultaneously handed off to the onboard control system. Initial experiments demonstrated that the MAV was able to successfully hover in "hands-off" mode for approximately 8–10 min before draining the battery (see Fig. 7). It should be noted that the aileron control surfaces remained in the neutral position (i.e., no deflection) throughout the flight. This was to purposefully allow torque roll so the MAV's bellycam could acquire panoramic footage of the flying area.

Another experiment was performed to contrast hovering under both manual and autonomous control. The metrics used were

1) duration of the hover before the FCS/human loses control;
2) stability of the aircraft while in hovering mode.

Fig. 7. MAV performing a *hands-off* autonomous hover in and urban structure.

A skilled human pilot was initially given control of the aircraft and was instructed to fly around a gymnasium in cruise configuration, transition from CTH flight, and an attempt to hover the aircraft for as long as possible. The video stills[1] on top of Fig. 8 show the pilot struggling to keep the fuselage vertical, but is able to keep the aircraft positioned over a small area. Out of a few trials, the human pilot was able to sustain a hover for several minutes before draining the battery. However, the aircraft's pitch and yaw angles oscillated significantly as the pilot tried to keep the aircraft in the vertical orientation. This is supported with a portion of the captured flight data, which is labeled *human-controlled*, in Fig. 9.

A second trial was conducted where the pilot was instructed to again fly in cruise configuration and manually transition from CTH flight. However, instead of trying to hover the aircraft manually, the pilot flicked a switch on the transmitter, which enabled the onboard control system. This time, the aircraft is fixed in a vertical position and able to hover for several minutes before exhausting the battery (see the bottom of Fig. 8). Again, the flight data were captured and a fraction of it is shown in Fig. 9. The length of the hover for the flight controller was comparable to that of the human; however, the FCS was able to achieve a higher margin of stability, as seen from the flight data.

B. Autonomous CTH Experiments

Another series of experiments were conducted to assess the autonomous CTH transition algorithm. The experiments are conducted outside an open field and inside an urban structure. In the autonomous hovering experiments, the aircraft is released close to the desired orientation. Therefore, the angular errors extracted from the hovering error quaternion are less than 30° in most cases. As such, the elevator and rudder control surfaces are rarely at full deflection. However, the pitch error extracted from the CTH error quaternion is approximately 90°. Implementing the control algorithm from Section III-B yields full elevator deflection from the start. However, a much higher derivative gain

[1]The video sequence shows three images extracted once a second for a period of 3 s. With the plane rotating at a rate of 0.25 r/s, this is enough to show two quarter rotations.

Fig. 8. (Top) Skilled human pilot hovers a fixed-wing aircraft in a small gymnasium and struggles to maintain a vertical orientation. (Bottom) Under autonomous control, the same aircraft is able to sustain a hover while remaining fixed in the vertical position.

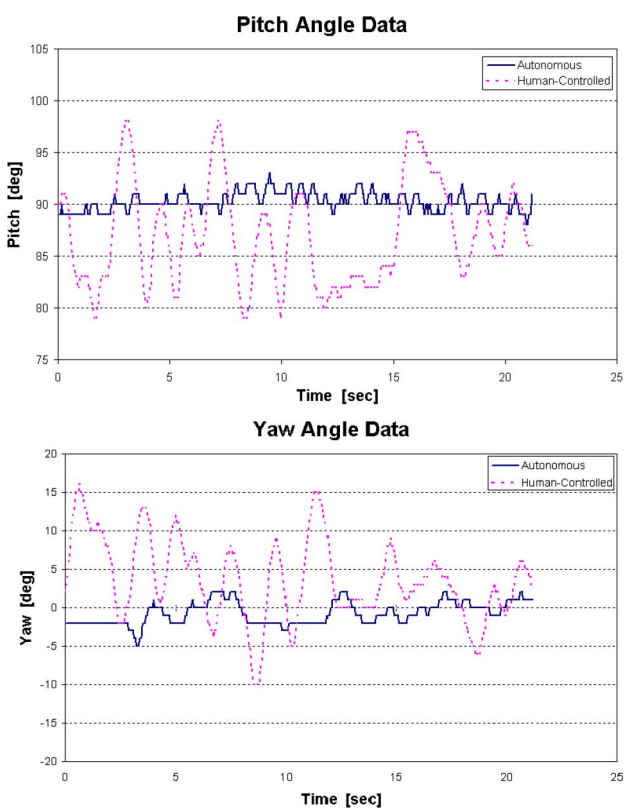

Fig. 9. Pitch and yaw angles captured during both human-controlled and autonomous hovering.

is used to kill the momentum as the aircraft approaches 90°, thus preventing overshoot.

An experiment was conducted outdoors in an open field. The human pilot loitered around the field in cruise mode and then flicked a switch on the transmitter to enable the onboard controller. This signaled the start of the autonomous transition and full elevator deflection was given by the controller. By substantially increasing the derivative gain, the rotation rate became the primary control factor. Therefore, the controller damped the rotation rate by cutting back on the elevator deflection, thus killing the momentum. The transition takes about a second and is shown in Fig. 10. During the experiments, the aircraft did not exceed a pitch angle of 90° when pitching up into the hovering flight mode.

Another CTH experiment was conducted inside a basketball gymnasium with a 25 ft ceiling. The procedure was similar to the outdoor flight tests in that the pilot manually flew the aircraft around the gymnasium in cruise mode. However, just before flicking the switch to enable the onboard attitude controller, the pilot had to precisely control the throttle. This was much different than the outdoor case where there was no risk of the aircraft crashing into the ceiling.

As the pilot enabled the autonomous flight controller, the plane began the transition to hover mode autonomously. However, it was noticed that the transition was not as smooth as it was outdoors, i.e., there was a significant amount of overshoot in the aircraft's pitch angle (see Fig. 11). The controller was still able to recover and stabilize the aircraft in the hovering orientation. The reason for the overshoot was that as the aircraft started gaining altitude, the pilot cut back significantly on the throttle to compensate. This resulted in a large decrease in airflow over the control surfaces and thus the elevator could not provide enough force to completely kill the momentum as the plane reached the hovering orientation.

C. Torque Roll Control

As originally thought, the torque roll did not affect the stability of the aircraft during a hover, that is, the MAV was still able to remain in the vertical position despite the rotations resulting from the motor torque. However, if the hybrid MAV was to be

Fig. 10. Transition from (left) cruise flight, through (center) the stall regime, and into (right) hover mode is achieved autonomously.

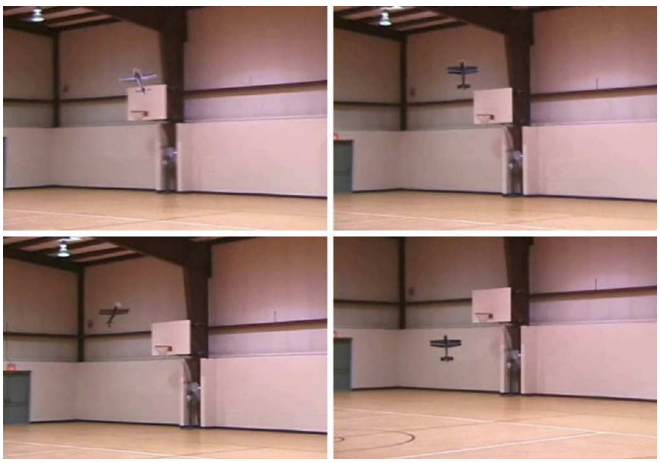

Fig. 11. (Top) Transition from cruise flight into hover mode is demonstrated inside an urban structure. (Bottom left) During the transition, the throttle is decreased to prevent the plane from colliding with the ceiling. This causes the aircraft to overshoot the vertical orientation. (Bottom right) The flight controller is able to recover and stabilize the MAV in its hovering orientation.

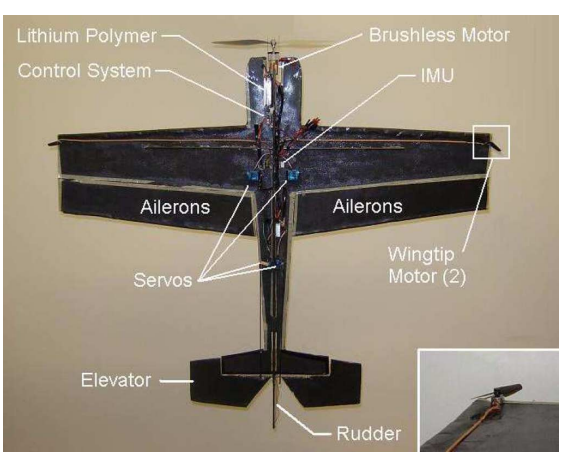

Fig. 12. Two dc motors are added on each wingtip to counter the motor's reactive torque. (Inset) Zoomed-in view of the wingtip motor.

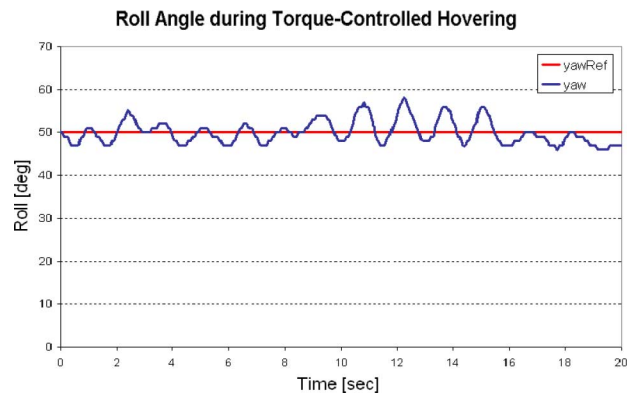

Fig. 13. Roll angle captured during autonomous hovering with torque roll control.

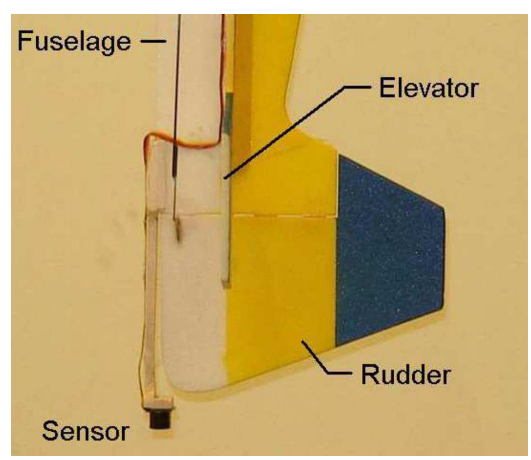

Fig. 14. Mount was created for the sonar sensor so that it would not interfere with the elevator and rudder control surfaces.

used in the field for surveillance and reconnaissance purposes, the view from the onboard wireless camera would have a dizzying effect as the plane was rotating at a rate of more than 20 rpm. Since the original aileron surface area did not create enough torque to counter the rotation when fully deflected, other alternatives had to be investigated. Also, to keep the cost and weight of the aircraft at a minimum, counter-rotating propellers were to be used as a last resort.

The first and most obvious approach was to increase the aileron surface area by lengthening them in the direction of the wing chord. However, this was not effective for several reasons. The first is that the propeller wash during a hover only flowed over approximately 40% of the ailerons. Second, a longer aileron when fully extended caused some airflow to completely miss the tail. This significantly affected attitude regulation during a hover. Finally, fully deflecting the ailerons created an adverse yaw effect that caused the airplane to drift when hovering.

Fig. 15. First two images in the above sequence show the hybrid MAV in a fully autonomous hover at a height of 36 in at 6 s apart. In the third image, a board was placed under the MAV's tail that caused the controller to adjust the MAV's height to 36 in above the board. This was used to show that a constant throttle setting was not used to perform altitude hold.

The second approach was to mount miniature dc motors with propellers on each wingtip. The motors were positioned to produce a thrust force in opposite directions, which generated a rotational force countering the motor torque (see Fig. 12). The wingtip motors are GWS EDP-20s, which provide 23 g of thrust with a 2510 direct drive propeller at 7.2 V. With the same error quaternion used in the autonomous hovering experiments, the angular error about the aircraft's x-axis was now incorporated into the flight controller. Using this parameter, proportional integral derivative (PID) control was implemented on the error. This determined the length of the PWM signal being output to the brushed speed controller.

Autonomous hovering experiments were conducted with torque roll control. Fig. 13 shows the torque-controlled condition in which the plane remains in a relatively constant orientation.

D. Altitude Hold

Without reliable global positioning system (GPS) signals in these environments, altitude control is a challenging task. Furthermore, the scope of the MAV's flying domain includes the insides of urban structures and thus altimeters are inefficient. Both ultrasonic and infrared sensors were investigated for altitude hold. The infrared sensors could not provide accurate and reliable measurements for distances larger than 0.5–1 m, and thus, ultrasonic sensing was chosen. The MaxSonar EZ-1 ultrasonic sensor was selected because of its 6-m range, 2.5-cm resolution, digital 20-Hz output, and 4.5-g weight.

The ultrasonic sensor had to be mounted on the hybrid prototype so that it would not be occluded when the elevator and rudder control surfaces were deflected. Furthermore, the mounting arm had to be designed so that it did not obstruct elevator and rudder deflection. The arm was created out of balsa wood and is shown in Fig. 14.

With the ultrasonic sensor securely mounted on the tail, a controller for fully autonomous hovering could now be implemented and tested. A PID controller with a setpoint height of 36 in was built upon the torque-controlled hovering algorithm from the previous subsection. A low-pass filter with a cutoff frequency of 5 Hz was implemented on the ultrasonic data to eliminate higher frequency noise. Furthermore, the throttle input was bounded to prevent the aircraft from losing or gaining altitude too quickly. The results of the experiment are shown in the first two images of Fig. 15. Furthermore, to show that the throttle was not set at a fixed position to balance the aircraft weight, a board is placed under the tail. This causes the FCS to adjust the aircraft's height to 36 in above the board, as seen in

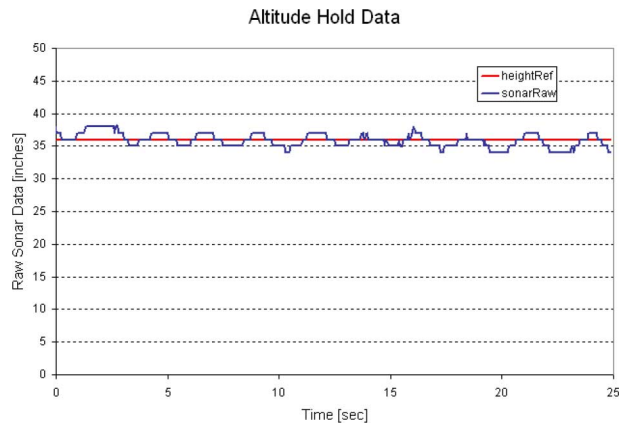

Fig. 16. Raw sonar data are plotted over the course of 20 s of fully autonomous hovering. The reference height value was set to 36 in. In the next 20 s, a board is placed under the aircraft to prove that the throttle is not set at a constant value to balance the aircraft weight.

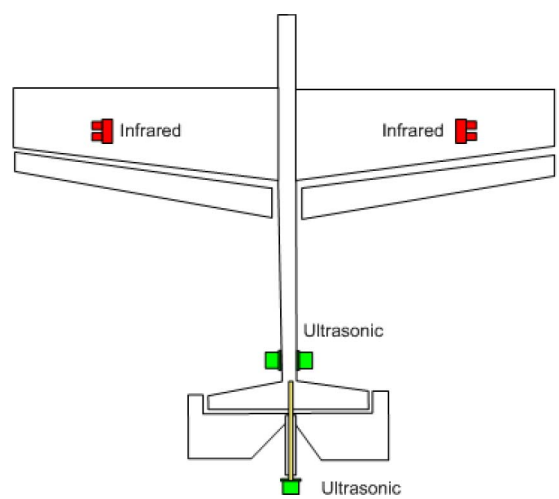

Fig. 17. Infrared sensor is mounted on each wing pointing out from the fuselage. Also, an ultrasonic sensor is mounted at the base of the fuselage pointing outward. This is so the propeller wash does not affect the sensor reading.

Fig. 18. Hybrid MAV autonomously follows the exterior wall of the building until detecting an open passageway. It then traverses the doorway to gather reconnaissance inside the building.

third image of Fig. 15. The ultrasonic data from the tail mounted sensor are shown in Fig. 16.

VI. Building Ingress and Reconnaissance Experiment

The hovering flight mode of the hybrid MAV allows it to maneuver in cluttered environments. Furthermore, the platform was designed to fit through small openings such as doorways. Using these characteristics and some additional sensing capabilities and control algorithms, an experiment is carried out where the MAV is able to detect a doorway and traverse it.

A. Sensor Suite

In addition to the IMU and tail-mounted ultrasonic sensor for altitude control, two MaxSonar EZ-1 ultrasonic sensors and two Sharp GP2Y0A02YK infrared sensors are incorporated into the sensor suite for wall following and doorway detection. Since the infrared sensors will mostly be used for doorway detection, the sensor inaccuracy at large distances will not be a factor. Furthermore, the disadvantages of both infrared and ultrasonic sensors can be improved by fusing the two sensing technologies together. This was shown in [4] where infrared and ultrasonic sensors were used in a complementary fashion to map out walls, doors, and windows of a residential basement.

Both the ultrasonic and infrared sensors have a minimum detection, or blind, distance. The blind distance for the ultrasonic and infrared sensors are 15 and 20 cm, respectively. The infrared sensors are not affected by the propeller wash and are therefore mounted on each wing. The ultrasonic sensors are mounted further away from the propeller at the base of the fuselage (see Fig. 17).

B. Navigational Controller

The control algorithm for building ingress and reconnaissance consists of three different control modes including wall following, stabilizing, and traversing. Each control mode sends different commands to the pitch and yaw control surfaces while the wingtip motors and main motor are continuously being adjusted to keep the MAV's roll angle and altitude constant, respectively.

Wall following mode incorporates data from both the infrared and ultrasonic sensors. Because ultrasonic sensors have a wide beam and are therefore inefficient at detecting edges or doorways, the infrared sensor is primarily responsible for determining the mode of the controller. The controller enters *wall following mode* if an obstacle is detected by both sensors and is less than 1.4 m away. The 1.4-m threshold was set based on the 1.5-m maximum detection distance of the infrared sensor. If the sensor detects an object within the 1.4-m threshold, it is assumed to be a wall. If the sensor does not detect anything, it will output a value corresponding to 1.5 m. In this case, the assumption is that there is an opening for the plane to transition through and the controller will then move to *stabilizing mode*. Once in *wall following mode*, the FCS still acquires data from both sensors but the control algorithm heavily weights the ultrasonic data to keep the MAV at a constant distance from the wall. This is because the ultrasonic sensor is much more accurate in measuring distance than the infrared sensor.

The second control mode is the *stabilizing mode,* which is initiated when the infrared sensor exceeds a distance threshold of 1.4 m for five counts. This is to allow the MAV extra translation time to get its entire frame past the wall and also to rule out any noisy measurements. The stabilizing control mode has two main functions. The first is to diffuse the forward momentum of the MAV so it dos not move past the doorway and the second is to get the aircraft back to the hovering orientation.

The final mode of the controller is the *traversing mode*. The traversing controller is just a simple reactive control algorithm used to yaw the aircraft into the detected opening, thus traversing the doorway. This process also acts as a failsafe to the wall following controller, that is, if the wall following controller

allows the aircraft to get more than 1.5 m away from the wall (i.e., an error of more than 75 cm), this will exceed the range of the infrared sensor causing the controller to incorrectly enter *stabilizing mode*. However, it will then enter *traversing mode,* which will just bring the MAV back toward the wall until it reenters the detection range of the sensors. This will then force the controller back into *wall following mode*.

C. Experiments

The experiment integrates quaternion algorithms, an FCS, attitude and altitude controllers, and a multiple mode, high-level controller used to demonstrate wall following. In addition, the navigational controller will also have to detect and move through a doorway to acquire situational awareness. The aircraft is released in a near-hovering attitude, and under full autonomous control, will follow the wall of the building. As it approaches the doorway, the controller will switch from wall following mode to stabilizing mode as discussed earlier. After it has regained stability in a hover, it will then transition to traversing mode. The MAV will move through the doorway and again stabilize itself in hovering mode. The results of the experiment are shown in Fig. 18.

VII. Conclusion

Patrolling subway tunnels and buildings demands a vehicle that can hover. Furthermore, other MAV missions such as gathering reconnaissance over a hill a few miles ahead requires endurance. Designing an aircraft for such missions demands a vehicle that is compact, able to fly for extended periods, and most importantly, is capable of hovering.

A fixed-wing MAV with hovering capabilities offers the benefits of stationary flight coupled with longer flight times. In addition, a "retrofit" system that can make existing MAVs hover would be attractive from both a cost and mission perspective (i.e., expand scope of capabilities). Furthermore, these unconventional flying environments are usually enclosed and thus degrade GPS signals. Therefore, onboard processing is preferred for autonomous operations. The 15-g processing and control system reads attitude information from the IMU at a 100-Hz rate and implements attitude control to autonomous hover the aircraft. Furthermore, a navigational control algorithm was developed to detect and traverse a doorway of a building.

The ultimate goal of this research was to use a holistic approach to develop a fully autonomous MAV to fly through tunnels and in and around urban buildings. Autonomous hovering and building ingress was a major milestone toward this, but the aircraft must also be able to perform other tasks autonomously. For example, the MAV's sensor suite and control system must be capable of obstacle detection in unstructured lighting, precise path planning, and localization. Collision avoidance can be accomplished by using optic flow to mimic flight stratagems of flying insects [12]. Furthermore, a scaled down version of the hybrid prototype is probably necessary in order to minimize risk when transitioning through small openings. This would also enable flight in tighter, more confined areas.

Acknowledgment

Any opinions, findings, and conclusions or recommendations expressed in this material are those of the author(s) and do not necessarily reflect the views of the National Science Foundation.

References

[1] G. Barrows, "Mixed-mode VLSI optic flow sensors for micro air vehicles," Ph.D. dissertation, Univ. Maryland, College Park, 1999.
[2] H. Choi, P. Sturdza, and R. M. Murray, "Design and construction of a small ducted fan engine for nonlinear control experiments," in *Proc. Amer. Control Conf.*, Baltimore, MD, 1994, pp. 2618–2622.
[3] R. Fearing, K. H. Chiang, M. Dickinson, D. L. Pick, M. Sitti, and J. Yan, "Wing transmission for a micromechanical flying insect," in *Proc. IEEE Int. Conf. Robot. Autom.*, San Francisco, CA, 2000, pp. 1509–1516.
[4] A. M. Flynn, "Combining sonar and infrared sensors for mobile robot navigation."
[5] W. E. Green and P. Y. Oh, "A MAV that flies like an airplane and hovers like a helicopter," in *Proc. IEEE/RSJ Int. Conf. Adv. Intell. Mechatron.*, Monterey, CA, 2005, pp. 699–704.
[6] W. E. Green, P. Y. Oh, and G. Barrows, "Flying insect inspired vision for autonomous aerial robot maneuvers in near-earth environments," in *Proc. IEEE Int. Conf. Robot. Autom.*, New Orleans, LA, 2004, pp. 2347–2352.
[7] T. Hamel, R. Mahony, and A. Chriette, "Visual servo trajectory tracking for a four rotor VTOL aerial vehicle," in *Proc. IEEE Int. Conf. Robot. Autom.*, Washington, DC, 2002, pp. 2781–2786.
[8] N. Hughes, Informal communication, Research Scientist, Analex Corporation, Fairfax, VA, Jan. 2006–Jan. 2007.
[9] J. Kellog *et al.*, "The NRL MITE air vehicle," presented at the 16th Bristol Int. Conf. Unmanned Air Vehicle Syst., Bristol, U.K., 2001.
[10] E. Lengyel, *Mathematics for 3D Game Programming and Computer Graphics*. Rockland, MA: Charles River Media, 2001.
[11] D. Ostrander, "An Engineer's Approach to Quaternions," *Internal Seminar at Martin Marietta*, 1986.
[12] M. V. Srinivasan, J. S. Chahl, K. Weber, S. Venkatesh, M. G. Nagle, and S. W. Zhang, "Robot navigation inspired by principles of insect vision," *Robot. Auton. Syst.*, vol. 26, pp. 203–216, 1999.
[13] J. R. Wertz, *Spacecraft Attitude Determination and Control*. Amsterdam, The Netherlands: Reidel, 1978.
[14] B. Wie, H. Weiss, and A. Arapostathis, "Quaternion feedback regulator for spacecraft eigenaxis rotations," *J. Guid., Control, Dyn.*, vol. 12, no. 3, pp. 375–380, 1989.

William E. Green received the B.Sc., M.Sc., and Ph.D. degrees in mechanical engineering from Drexel University, Philadelphia, PA, in 2002, 2004, and 2007, respectively.

He is currently a Design Engineer with the Avionics and Software Department, Alliant Techsystems (ATK), Minneapolis, MN. His current research interests include aerial robotics, mechatronics, and computer vision.

Paul Y. Oh received the B.Eng. degree from McGill University, Montreal, QC, Canada, in 1989, the M.Sc. degree from Seoul National University, Gwanak, Seoul, Korea, in 1992, and the Ph.D. degree from Columbia University, New York City, in 1999.

He is currently a Professor with the Mechanical Engineering Department, Drexel University, Philadelphia, PA, where he is also the Director of the Drexel Autonomous Systems Laboratory.

Prof. Oh received fellowships from the NASA Jet Propulsion Laboratory (2002) and the Naval Research Laboratory (2003), and he received the National Science Federation CAREER award (2004), and the Society of Automotive Engineers (SAE) Ralph Teetor Award for Engineering Education Excellence (2005). He was also named a Boeing Welliver Fellow in 2006. He is also the Founding Chair of the IEEE Technical Committee on Aerial Robotics and Unmanned Air Vehicles.